ISSN 0915-633X

NATIONAL INSTITUTE FOR FUSION SCIENCE

Three Dimensional Studies of Helical Equilibria and Magnetic Surface Breaking Due to the Finite Beta Effect

T. Hayashi, T. Sato and A. Takei

(Received – Oct. 26, 1989)

NIFS-7 Feb. 1990

RESEARCH REPORT
NIFS Series

NAGOYA, JAPAN

THREE DIMENSIONAL STUDIES OF HELICAL EQUILIBRIA AND MAGNETIC SURFACE BREAKING DUE TO THE FINITE BETA EFFECT

Takaya Hayashi and Tetsuya Sato

National Institute for Fusion Science,

Nagoya 464-01, Japan

Akira Takei

Institute for Fusion Theory, Hiroshima University,

Hiroshima 730, Japan

Abstract

Three dimensional equilibrium and breaking of magnetic surfaces due to the finite beta effect in a l=2 heliotron/torsatron configuration are studied by using a newly developed three-dimensional equilibrium code. The breaking is significantly suppressed as γ_c (pitch parameter) becomes smaller. An inward shift of the plasma by using the vertical field and elliptic (vertical) shaping using the quadrupole field can also suppress the breaking.

Keywords

helical system, stellarator, equilibrium, magnetic surface, finite beta effect, ergodic region, computer simulation, three dimensional equilibrium code, magnetic surface breaking

I. Introduction

One of the main targets of the present (ATF)[1] and the next step (Large scale Helical System)[2] helical devices is to obtain a high beta plasma, such as $\bar{\beta} \geq 5\%$, where $\bar{\beta}$ denotes the averaged value of β. It is known, however, that a non-axisymmetric toroidal finite beta equilibrium does not necessarily regularly nest magnetic surfaces.[3-7]

As a measure to define the equilibrium beta-limit of helical systems, the amount of the shift of the magnetic axis due to a finite pressure effect (Shafranov shift) $\Delta_s(\beta)$ is often used, specifically, $\Delta_s(\beta) < \frac{\bar{a}_p}{2}$, where $\bar{a}_p$ is the average plasma minor radius.[1] However, we should be careful against the breaking of magnetic surfaces in an equilibrium caused by the symmetry-breaking of the configuration, which is specific to a non-axisymmetric torus. In a helical system, the outside of the outermost magnetic surface is the region with magnetic islands or ergodic field lines even in the vacuum field. What should be analyzed is, therefore, how largely the ergodic region expands in a finite beta equilibrium. The breaking of magnetic surfaces (appearance of magnetic islands) in the finite beta equilibrium is caused by the plasma current which induces error poloidal magnetic fields in resonance with rational magnetic surfaces.

The plasma current (especially the field-aligned current or Pfirsch-Schluter current) is important in two points in a helical equilibrium. One is its dipole moment that generates the vertical field, which induces the shift of the magnetic axis. The other is the generation of the resonant error fields mentioned above. A number of poloidal modes m are included in the error field due to the toroidal effect. In the case of an axisymmetric torus, the toroidal mode number n of the error fields is limited to be 0. Therefore they do not resonate with any rational surfaces except for a very special case with

the rotational transform $\iota=0$. On the other hand, in the case of a non-axisymmetric helical torus, n can be harmonics of the pitch period number M, thus some error fields can satisfy the resonant condition $\iota=\frac{n}{m}$ inside the plasma region.

In the finite beta helical equilibrium it may be conceived that, when β is rather low, the plasma automatically chooses such a configuration that the current distribution is suitably adjusted through the deformation of the shape of the magnetic surfaces. As a result, an equilibrium is reached (or very closely reached) in which the integrated error fields do not generate islands by resonant effects, and at the same time, $j\times B=\nabla p$ is satisfied everywhere self-consistently. It is also conceived that, when β becomes rather high, a transition occurs at which an equilibrium allowing the generation of islands can be a lower energy state than the one keeping clear magnetic surfaces by a complicated current distribution, thus the breaking of magnetic surfaces occurs.

A number of computer codes have been developed and actively used to obtain and evaluate three dimensional (3D) helical equilibria. Some examples of them are BETA[8] and VMEC[9], which use Lagrangean coordinates, and Chodura–Schluter[10] and NEAR[11], which use Eulerian coordinates. However, these codes assume the existence of clearly nested magnetic surfaces, explicitly or implicitly. Therefore, even though the breaking of magnetic surfaces in finite beta helical equilibria is a crucial problem, it remains not to be clarified. Several efforts have been addressed to evaluate numerically the breaking so far (for example, ref.12). This paper describes results of another approach[13].

In the present study, we analyze quantitatively 3D equilibria and the magnetic surfaces breaking due to finite beta effect for a toroidal $l=2$ heliotron/torsatron configuration with a rather low aspect ratio. For this pur-

pose we have developed a new 3D magneto-hydrodynamic computer code (HINT) which obtains a currentless helical equilibrium by a relaxation method (an initial value method) with a fourth-order accuracy scheme in a free-boundary Eulerian coordinate system. The coordinate system rotates with the same pitch as the helical coil. The poloidal boundary is assumed to be rectangler and a perfect conductor; the plasma pressure is null there. The calculation region covers the outermost magnetic surface and a part of the outer ergodic vacuum region. Since the details of the numerical scheme are described in other papers[13,14,15], we do not reproduce them here.

II. Vacuum Field

Before going to the finite beta equilibrium, we describe the characteristic of the vacuum field in this section. We examine a configuration of $M=10/l=2$, and we assume that the major radius of the center of the helical coil $R_c=4.0(m)$ in the following. The coil current is approximated by a thin filament. The axisymmetric external poloidal fields are expressed by coefficients of the multipole expansion at the center of the helical coil. We examine the independent control of magnetic surfaces by the external vertical field component and the quadrupole component.

A. Vertical field B_v control

Shown in Fig.1 (a)-(d) are the vacuum magnetic surfaces of a configuration with $\gamma_c=1.21$ (the minor radius of the helical coil $a_c=0.97(m)$) for four cases of the position of the magnetic axis where the external uniform vertical field B_v is changed; $\gamma_c \equiv \frac{M}{l}\frac{1}{A_c}$ and $A_c \equiv \frac{R_c}{a_c}$ is the coil aspect ratio. The figure shows the cross section at the toroidal angle $\phi=0$. The radial posi-

tion of the magnetic axis corresponds to R_0=4.01,3.89,3.76, and 3.63(m), respectively. (Precisely speaking, the magnetic axis has the structure of the helical axis, although the scale is small. Here, R_0 is described by the position of the averaged center of the "small" helical axis.) Excessive inward shift of the magnetic axis practically gives rise to serious problems, such as an onset of instability due to the lack of the magnetic well, or an insufficient clearance between the plasma boundary and the helical coil when the finite width of the helical coil is taken into account. However, in this paper we examine the effect of the shift for a rather wide range in order to investigate the tendency of the characteristic of the equilibrium solutions.

Corresponding change of the rotational transform versus Δ_{shift} is plotted in Fig.2, where Δ_{shift} is the amount of the shift of the magnetic axis measured from the coil center R_c (=4(m)), and ι_0 and ι_a are the rotational transform at the magnetic axis and the plasma boundary, respectively. The minimum of ι_0 ($\Delta_{shift}\approx-0.15(m)$) corresponds to the case in which the position of the magnetic axis almost coincides with the center of other surfaces.

The average minor radius of the outermost magnetic surface $\bar{a}_p$ versus Δ_{shift} is plotted in Fig.3. $\bar{a}_p$ shrinks when the magnetic axis is shifted either excessively outward or inward. Also plotted in Fig.3 is $\bar{a}_p$ for a configuration with γ_c=1.31. $\bar{a}_p$ remarkably increases when γ_c is increased.

The radial profile of the magnetic well $W(\bar{r})$ for the γ_c=1.21 configuration is plotted in Fig.4(a) for the different values of B_v. Here, W is defined as $W(\bar{r})\equiv\frac{U(0)-U(\bar{r})}{U(0)}\times 100$ (%) where the specific volume $U=(\frac{1}{N})\int_N \frac{dl}{B}$ is evaluated on a surface, $U(0)$ denotes the value on the magnetic axis and $U(\bar{r})$ denotes the value on the magnetic surface with average radius $\bar{r}$. A local magnetic well exists when $dW/d\bar{r}$ is positive. The hill in-

creases as the magnetic axis is shifted inward.

Figure 4(b) shows the radial profile of $\sigma(\int_{1pitch}\frac{dl}{B})$, which denotes the variation of $\int_{1pitch}\frac{dl}{B}$ on a magnetic surface, namely,

$$\frac{<(\int\frac{dl}{B})^2> - <(\int\frac{dl}{B})>^2}{<(\int\frac{dl}{B})>^2}$$

where <> denotes an average on a surface. The variation is directly related with the magnitude of $j_{//}$ (Pfirsch-Schluter current) through the relation that

$$\frac{j_{//}}{B}\approx -\frac{2}{\iota}\frac{dp}{dF_t}\Delta(\int_{1pitch}\frac{dl}{B})$$

where

$$\Delta(\int_{1pitch}\frac{dl}{B})\equiv\int_{1pitch}\frac{dl}{B}-<\int_{1pitch}\frac{dl}{B}>.$$

The variation σ, as well as the magnetic well W, changes significantly as the shift of the magnetic axis. It rapidly and monotonically decreases with inward shift.

B. Quadrupole field B_q control

The quadrupole component of the external field B_q controls the ellipticity of the magnetic surface. Figure 5 (a)-(c) show different shape of magnetic surfaces for three cases of B_q for the confiruration with γ_c=1.31 and R_0=4.0(m). The magnitude of the external quadrupole field B_q is described by a ratio on that of the quadrupole field generated by the helical coil. Therefore, for the case (c) in Fig.5, for which B_q=−100(%), the quadrupole field of the helical coil is cancelled by the external B_q near the coil center, thus the averaged shape of the magnetic surfaces is almost a circle. The correspond-

ing profiles of ι, the magnetic well W, and $\sigma(\int_{1pitch}\frac{dl}{B})$, are plotted in Fig.6. As the averaged magnetic surface becomes prolate (vertically elliptic), the depth of the magnetic well, as well as ι_0, reduces. The magnitude of $\sigma(\int_{1pitch}\frac{dl}{B})$ also reduces, but not as significantly as for the case of B_v control shown in Fig.4 (b).

C. γ_c dependence

The plasma aspect ratio decreases as γ_c is increased, as is shown in Fig.3. The profiles of ι, the magnetic well W, and $\sigma(\int_{1pitch}\frac{dl}{B})$, are plotted in Fig.7 for two cases of γ_c (γ_c=1.21 and 1.31, and for both cases, R_0=3.9(m), and B_q=0). As γ_c is increased, $\iota(\bar{r})$ prominently decreases, and the well depth increases. However, there is no remarkable change in $\sigma(\int_{1pitch}\frac{dl}{B})$.

III. Finite Beta Equilibrium

An equilibrium calculated by the HINT code is compared with that by the VMEC code[16] for the same configuration (γ_c=1.34, R_0=4.0(m), and the pressure profile is $p(\psi_p)=p_0(1-\psi_p)^2$) in Fig.8, where the shift of the magnetic axis $\Delta_s(\beta)$ normalized by the initial major radius $R(0)$ is plotted versus β at the magnetic axis. The agreement is fairly good.

In Fig.9, the deformation of the shape of magnetic surfaces accompanying an increase of β is shown for the case with γ_c=1.21 and R_0=3.76(m). The pressure profile is assumed to be $p(\psi_t)=p_0(1-\psi_t)^2$, where ψ_t is the toroidal magnetic flux normalized to be 1.0 at the plasma boundary. The pressure profile is kept while the breaking of magnetic surfaces, as will be

described in Section IV, does not occur. We stop increasing β in the equilibrium calculation when the breaking of magnetic surfaces due to finite beta effect becomes prominent. Clear magnetic surfaces are kept up to relatively high $\bar{\beta}$ ($\bar{\beta}\approx 6\%$) in this case. The corresponding profiles of the plasma pressure and the toroidal current are shown in Fig.10.

The change of profiles of the rotational transform, the magnetic well, and $\sigma(\int_{1pitch}\frac{dl}{B})$ with β is plotted in Fig.11 (a)-(d) for the cases with $\gamma_c=1.21$ and $R_0=4.01,3.89,3.76$, and $3.63(m)$. The rotational transform at the magnetic axis ι_0 increases as $\bar{\beta}$ is increased, and that on the plasma boundary ι_a decreases for the "standard" case such as (a) and (b), namely, $R_0=4.01$ and $3.89(m)$. On the contrary, for strongly inwardly-shifted cases such as (c) and (d), for which the magnetic axis is located on the inner half side of the poloidal cross section of the outermost magnetic surface, ι_0 decreases as $\bar{\beta}$ is increased. This difference may be due to the difference of the change of the geometrical shape of magnetic surfaces near the magnetic axis when $\bar{\beta}$ is increased. The magnetic well is rapidly deepened for every case as $\bar{\beta}$ is increased, which causes self-stabilization if sufficiently deepened. Compared with the changes of the rotational transform and the well, the values of $\sigma(\int_{1pitch}\frac{dl}{B})$ do not significantly change when $\bar{\beta}$ is increased, and keep the characteristic of the vacuum field that its value is smaller as the inward shift is larger.

The total flux of the positive component of the toroidal current, which is equal to that of the negative component since a currentless equilibrium is obtained, is plotted versus $\bar{\beta}$ in Fig.12. The flux becomes smaller for the inwardly shifted case.

The shift of the magnetic axis due to beta effect $\Delta_s(\beta)$ normalized by the initial average plasma radius $\bar{a}_p$ is plotted in Fig.13. For this configuration,

the equilibrium $\bar{\beta}$ limit is determined by the condition of $\Delta_s(\beta)<\frac{\bar{a}_p}{2}$, except for the cases with R_0=4.01 and 3.95(m).

IV. Breaking of Magnetic Surfaces

In this section we discuss the appearance of magnetic islands in a finite beta equilibrium, and ergodization of magnetic surfaces as a result of the overlapping of islands. The value of $\bar{\beta}$ at which the breaking occurs depends on many physical parameters. In this paper we examine the breaking in a rather practical way. Namely, we examine its dependence on γ_c and the external field B_v and B_q.

A. Island Formation and Ergodization

Let us study with the first example with a configuration for γ_c=1.31 and R_0=3.95(m). The vacuum field has clear magnetic surfaces up to the outermost surface. In Fig.14(a), magnetic surfaces of this configuration for $\bar{\beta}$=1.8% are shown. Clearly nested magnetic surfaces are kept perfectly up to the outermost magnetic surface at this low beta equilibrium, although the position of the magnetic axis has already shifted significantly from that for the vacuum field. However, as $\bar{\beta}$ is increased up to 2.8 %, as is shown in Fig.14(b), magnetic islands appear on the plasma boundary. The resonant condition of the island can be written as $\iota=kM/m$, where m is the poloidal mode number, and k is any integer. In order to identify the mode number of each island, the corresponding resonant position (for the fundamental case k=1) in the ι profile is also plotted in Fig.14(b). (The islands with only odd number of m are observed in Fig.14(b). But note that it is accidental; it depends on the choice of the start positions of traced field lines. Islands with

even m, such as $m=10,12,etc$, actually exist between odd islands.) When β is further increased, the width of the island increases. Meanwhile, as is shown in Fig.14(c) for $\bar{\beta}=3.5\%$, ergodization of magnetic surfaces is induced by the overlapping of islands.

In this case, the breaking of magnetic surfaces appears at lower $\bar{\beta}$ than that at which the shift of the magnetic axis exceeds $\frac{\bar{a}_p}{2}$, thus the occurence of the breaking imposes more severe equilibrium β limit.

B. Numerical Check

In order to confirm that the appearance of islands, such as observed in Fig.14 (b) and (c), is not due to a numerical error, but due to a physical mechanism, we make two kinds of check. The first one is the convergence check, where calculations with two different mesh sizes ($73\times73\times29$ and $49\times49\times21$ for half pitch period) are compared for the configuration with $\gamma_c=1.21$ and $R_0=3.95$. The results are shown in Fig.15 for $\bar{\beta}=2.5\%$ and 3.5%. The second one is to check a numerical error arising on the boudary, where calculations with two different boudary positions (the size of poloidal cross section is $1.0(m)\times1.8(m)$ and $1.4(m)\times2.6(m)$) are compared in Fig.16 for $\bar{\beta}=2.1\%$ and 3.2% . In both checks the results are very similar, which supports that the results are physical.

C. Suppression of Breaking by Control of B_v, B_q, and γ_c

The extent of the breaking of magnetic surfaces is summarized in Fig.17,18 and 19. Figure 17 is for the case with $\gamma_c=1.21$ for different positions of the vacuum magnetic axis when B_v is changed, where ○ denotes that clear magnetic surfaces are kept, Δ denotes the appearance of islands, and × denotes that the width of the ergodized plasma boundary is more than about

.25 of $\bar{a}_p$. The breaking is remarkably improved by the inward shift. Figure 18 again shows results for the B_v control, but for γ_c=1.31. The same tendency of improvement by the inward shift is observed. Comparing Fig.17 and 18, it is noted that the breaking is significantly reduced, in general, when γ_c is decreased, namely, the coil aspect ratio is increased.

Similarly, Fig. 19 (a)(b) shows the effect of B_q control for the case with γ_c=1.31, (a) for R_0=3.8 and (b) for R_0=4.0. The breaking is improved by controlling the shape vertically elliptic in average.

V. Discussion and Summary

Several discussions have so far been made on the fragility of the vacuum field of the low aspect ratio heliotron/torsatron configuration[17,18,19] . Especially it is pointed out that clearly nested magnetic surfaces can be restored in the outer ergodic region by properly controlling the winding law (the modulation) of the helical coil, or by controlling the coil currents of several pairs of axisymmetric poloidal field coils (equivalently, the multipole components of the external field, such as the dipole or quadrupole components) . In fact, significant effects of multipole components of the external field on the vacuum magnetic surfaces are also observed in this work. Let us here compare the fragility of magnetic surfaces of the vacuum field with the fragility for the non-zero pressure case. For this purpose, we define the fragility of the vacuum field by the average minor radius of the outermost surface $\bar{a}_p$.

First, we examine the effect of the vertical field B_v on the fragility. As is shown in Fig.3, $\bar{a}_p$ increases when the magnetic axis is shifted inwards in the range of $\Delta_{shift} \geq -0.2(m)$. In the meantime, as we have seen in Fig.17 or 18, the fragility for the finite pressure case is significantly improved with the

inward shift of the magnetic axis. Thus, we can say that the improvement in the vacuum fragility in this range (i.e., $\Delta_{shift} \geq -0.2(m)$) has the similar tendency with that for the finite pressure case. When the inward shift exceeds $-0.2(m)$, however, a_p of the vacuum field decreases. On the other hand, the improvement for the finite pressure case continues even when the inward shift goes beyond $-0.2(m)$.

Next, we go on to the effect of the quadrupole field B_q on the fragility. We have observed a similar tendency of the improvement in the fragility both for the vacuum (see Fig.6) and the finite pressure case (Fig.19) . Namely, the vertically elongated configuration is favorable for both cases.

Finally, we shall examine the effect of γ_c . The fragility is deteriorated for the vacuum field when γ_c is decreased, as is shown in Fig.3. On the contrary, the fragility for the finite pressure case is significantly improved when γ_c is decreased, as can be observed by comparing Fig.17 and Fig.18. This indicates that the tendency is completely opposite for the change of γ_c .

These investigations concludes that the tendency of the improvement in the fragility does not always the same for the vacuum and finite pressure cases.

The main conclusion of the paper is that we need to analyze the breaking of boundary magnetic surfaces due to the finite beta effect in evaluating the equilibrium beta limit of a helical system, in addition to the usual standard of the Shafranov shift $\Delta_s(\beta) < \frac{\bar{a}_p}{2}$.

We have found several methods to suppress the breaking of magnetic surfaces. The breaking is reduced

(a) significantly as γ_c becomes smaller,

(b) as the magnetic axis is shifted inwardly by controlling B_v,

(c) as the plasma is vertically and elliptically shaped by adding B_q component.

The inward shift of the magnetic axis in a low aspect ratio heliotron/torsatron is favorable from another point of view; the significant improvement in the amount of loss of particle orbits[2], if the shift is not excessive. However, a further careful study on the stability, as well as the clearance between the plasma and the wall, is necessary to determine the limit of inward shift.

Acknowledgements

We would like to thank Prof.K.Nishikawa for continuous encouragement. We are grateful to Dr.J.Todoroki, Dr.Y.Nakamura and Dr.M.Wakatani for discussions on the equilibria code. We are also grateful to Dr.J.Nuhrenberg for valuable discussions on the pressure driven current. This research was supported by the grant-in-aid for the fusion research by the Ministry of Education, Science and Culture in Japan.

REFERENCES

[1] B.A.Carreras, H.R.Hicks, J.A.Holme, V.E.Lynch, L.Garcia, J.H.Harris, T.C.Hender, and B.F.Masden, Phys. Fluids **26**, 3569(1983).

[2] A.Iiyoshi, *in Proceedings of the US-Japan Workshop on New Generation Experiments and Reactors* (Kyoto University, Kyoto, 1988), Vol.1, p.11

[3] S.Hamada, Nucl. Fusion **2**, 23 (1962).

[4] A.H.Reiman and A.H.Boozer, Phys. Fluids **27**, 2446 (1984).

[5] J.R.Cary and M.Kotschenreuther, Phys. Fluids **28**, 1392 (1985).

[6] C.C.Hegna and A.Bhattacharjee, Phys. Fluids B **1**, 392 (1989).

[7] A.H.Reiman, N.Pomphrey, and A.H.Boozer, Phys. Fluids B **1**, 555 (1989).

[8] F.Bauer, O.Betancourt and P.Garabedian, *A Computational Method in Plasma Physics* (Springer-Verlag, New York, 1978) ; F.Bauer, O.Betancourt and P.Garabedian, *Magnetohydrodynamic Equilibrium and Stability of Stellarators* (Springer-Verlag, New York, 1984)

[9] S.P.Hirshman and D.K.Lee, Comput. Phys. Commun. **39**, 161 (1986).

[10] R.Chodura and A.Schluter, J. Comput. Phys. **41**, 68 (1981).

[11] T.C.Hender, B.A.Carreras, L.Garcia, J.A.Rome and V.E.Lynch J.Comput.Phys. **60**, 76 (1985).

[12] H.S.Greenside, A.H.Reiman, and A.Salas, J. Comput. Phys. **81**, 102 (1989).

[13] K.Harafuji, T.Hayashi and T.Sato, J. Comput. Phys., **81**, 169 (1989).

[14] T.Hayashi, *in Proceedings of the Joint Varenna-Lausanne International Workshop on Theory of Fusion Plasma,* edited by J.Vaclavik, F.Troyon, and E.Sindoni (CRPP-EPFL, Lausanne, 1989), p.11

[15] R.Horiuchi and T.Sato, Phys. Fluids B **1**, 581 (1989).

[16] Y.Nakamura and M.Wakatani, private communication.

[17] J.R.Cary and J.D.Hanson, Phys.Fluids **29**, 2464 (1986).

[18] B.A.Carreras, N.Dominguez, L.Garcia, J.R.Cary, J.D.Hanson, and A.P.Navarro, Nucl.Fusion **28**, 1195 (1988).

[19] Y.Nakamura, private communication.

FIGURE CAPTIONS

Fig.1 Vacuum magnetic surfaces of the $M=10/l=2$ configuration with $\gamma_c=1.21$ and $R_c=4.0(m)$ for four cases of the radial position of the magnetic axis by a control of the vertical field B_v .

Fig.2 The rotational transform at the magnetic axis ι_0 and that on the boundary ι_a versus the radial position of the magnetic axis Δ_{shift} for the vacuum field of the same configuration with Fig.1. Δ_{shift} is measured from the central position of the helical coil $R_c=4(m)$.

Fig.3 The average plasma radius $\bar{a}_p$ versus Δ_{shift} for $\gamma_c=1.21$ and 1.31.

Fig.4 The radial profile of (a) the magnetic well $W(\bar{r})$ and (b) the variation of $\int_{1pitch} \frac{dl}{B}$ for the vacuum field of the $\gamma_c=1.21$ configuration with five different values of B_v.

Fig.5 Vacuum magnetic surfaces of the $M=10/l=2$ configuration with $\gamma_c=1.31$ and $R_0=4.0(m)$ for three cases of the elliptic shaping by a control of the quadrupole field B_q.

Fig.6 The radial profile of (a) ι (b) W and (c) the variation of $\int_{1pitch} \frac{dl}{B}$ for the vacuum field of the $\gamma_c=1.31$ configuration with three different values of B_q corresponding to Fig.5.

Fig.7 The radial profile of (a) ι (b) W and (c) the variation of $\int_{1pitch} \frac{dl}{B}$ for two cases of γ_c, where $R_0=3.9(m)$ and $B_q=0$.

Fig.8 Comparison of a finite beta equilibrium calculation by the VMEC code and by the HINT code, where the radial shift of the magnetic axis is plotted versus β at the magnetic axis.

Fig.9 The deformation of the shape of magnetic surfaces accompanying an increase of β for the γ_c=1.21 and R_0=3.76(m) configuration. Regularly nested magnetic surfaces are kept up to relatively high $\bar{\beta}$ ($\bar{\beta}\approx 5-6\%$) in this case.

Fig.10 Contour plots of the plasma pressure (upper panel) and the toroidal plasma current (lower panel) corresponding to Fig.9. One dimensional profile at the midplane is plotted for each contour.

Fig.11 The change of profiles of ι,W and the variation of $\int_{1pitch} \frac{dl}{B}$ with $\bar{\beta}$ for the γ_c=1.21 cofiguration with (a) R_0=4.01(m), (b) R_0=3.89(m), (c) R_0=3.76(m), and (d) R_0=3.63(m).

Fig.12 The total flux of the positive component of the toroidal current versus $\bar{\beta}$.

Fig.13 The shift of the magnetic axis $\Delta_s(\beta)$ normalized by the initial average plasma radius $\bar{a}_p$ versus $\bar{\beta}$.

Fig.14 Magnetic surfaces of the γ_c=1.31 configuration (a) for $\bar{\beta}$=1.8%, (b) for $\bar{\beta}$=2.8% (each island is identified with the corresponding resonant position), and (c) for $\bar{\beta}$=3.5%.

Fig.15 Numerical check of the appearance of the breaking of magnetic surfaces I : Calculations with two different mesh sizes (73×73×29 and 49×49×21) for $\bar{\beta}$=2.5% and $\bar{\beta}$=3.5% for the same γ_c=1.21 configuration with R_0=3.95(m).

Fig.16 Numerical check of the appearance of the breaking of magnetic surfaces II : Calculations with two different boundary positions ($1.0(m)\times1.8(m)$ with $49\times49\times21$ mesh and $1.4(m)\times2.6(m)$ with $73\times73\times29$ mesh) for the same $\gamma_c=1.21$ configuration with $R_0=3.95(m)$.

Fig.17 Summary of the extent of the breaking of magnetic surfaces for the $\gamma_c=1.21$ configuration with five different Δ_{shift} (B_v control) : ○ denotes that clear magnetic surfaces are kept, Δ denotes the appearance of prominent islands, and × denotes that the width of the ergodized plasma boundary is more than about .25 of $\bar{a}_p$.

Fig.18 Similar plot to Fig.17, but for the $\gamma_c=1.31$ configuration.

Fig.19 Similar plot to Fig.17, but for the B_q control in the $\gamma_c=1.31$ configuration (a) with $R_0=3.8(m)$ and (b) with $R_0=4.0(m)$.

$\phi = 0°$

$\gamma_c = 1.21$

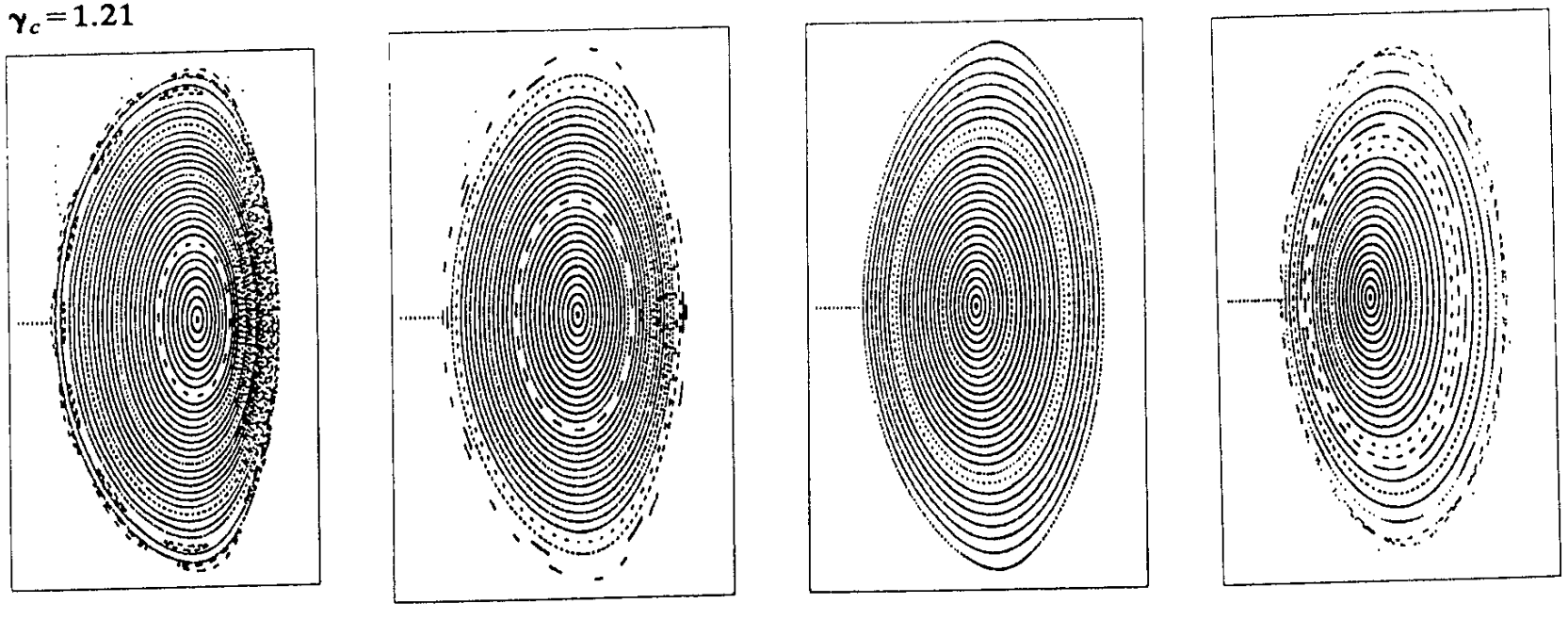

(a) $R_0 = 4.01(m)$ (b) $R_0 = 3.89(m)$ (c) $R_0 = 3.76(m)$ (d) $R_0 = 3.63(m)$

Fig. 1

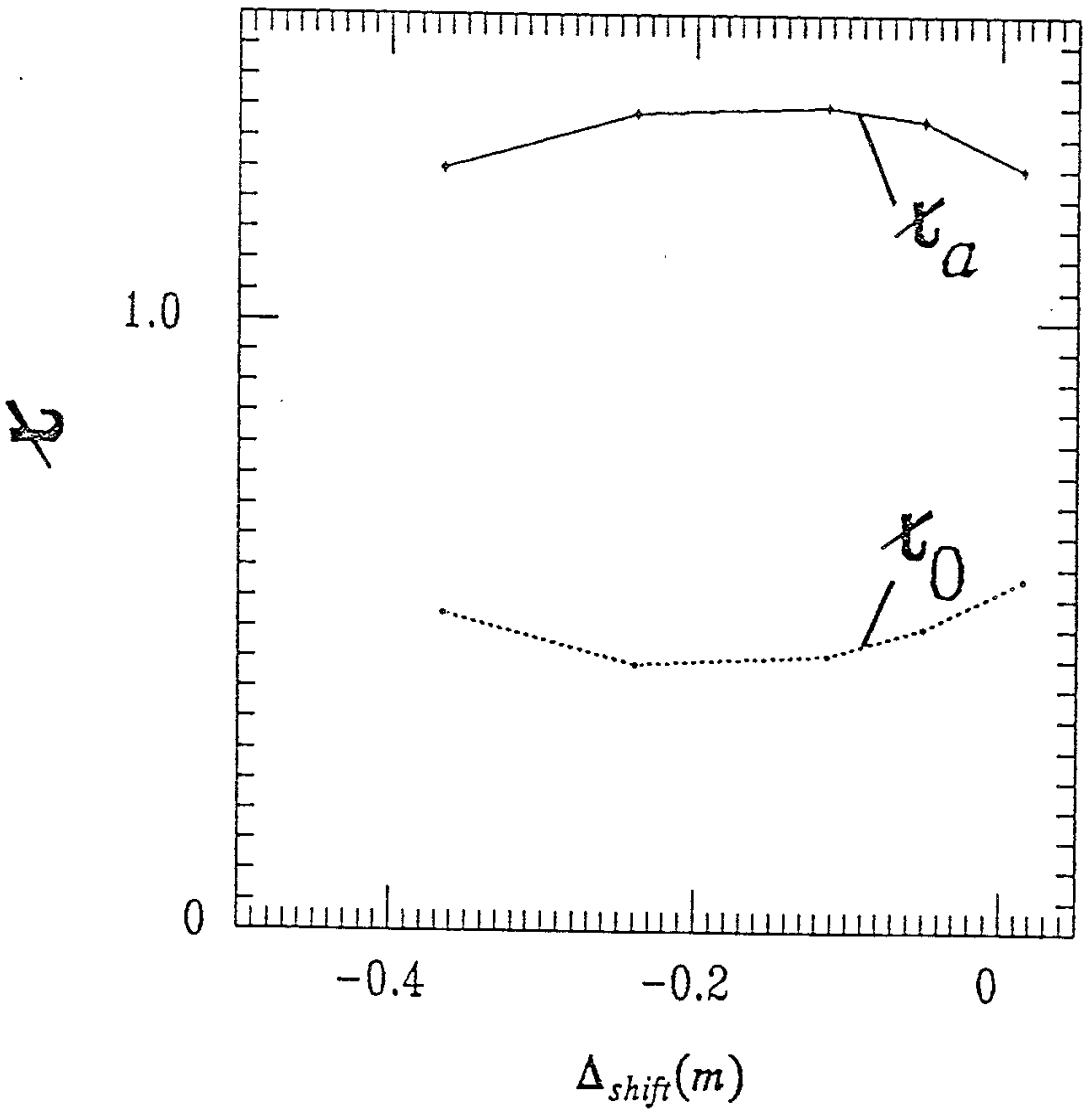

Fig.2

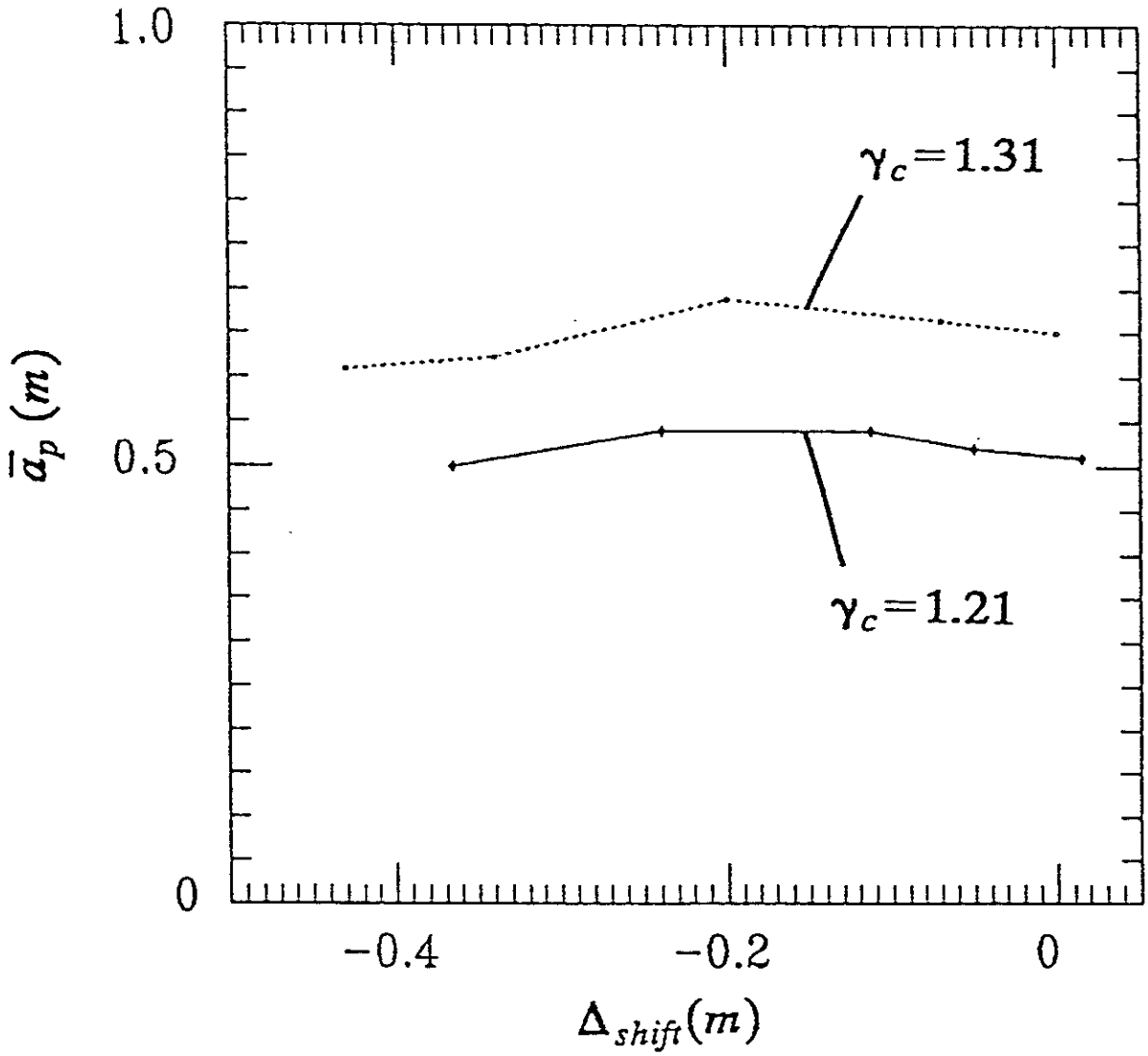

Fig.3

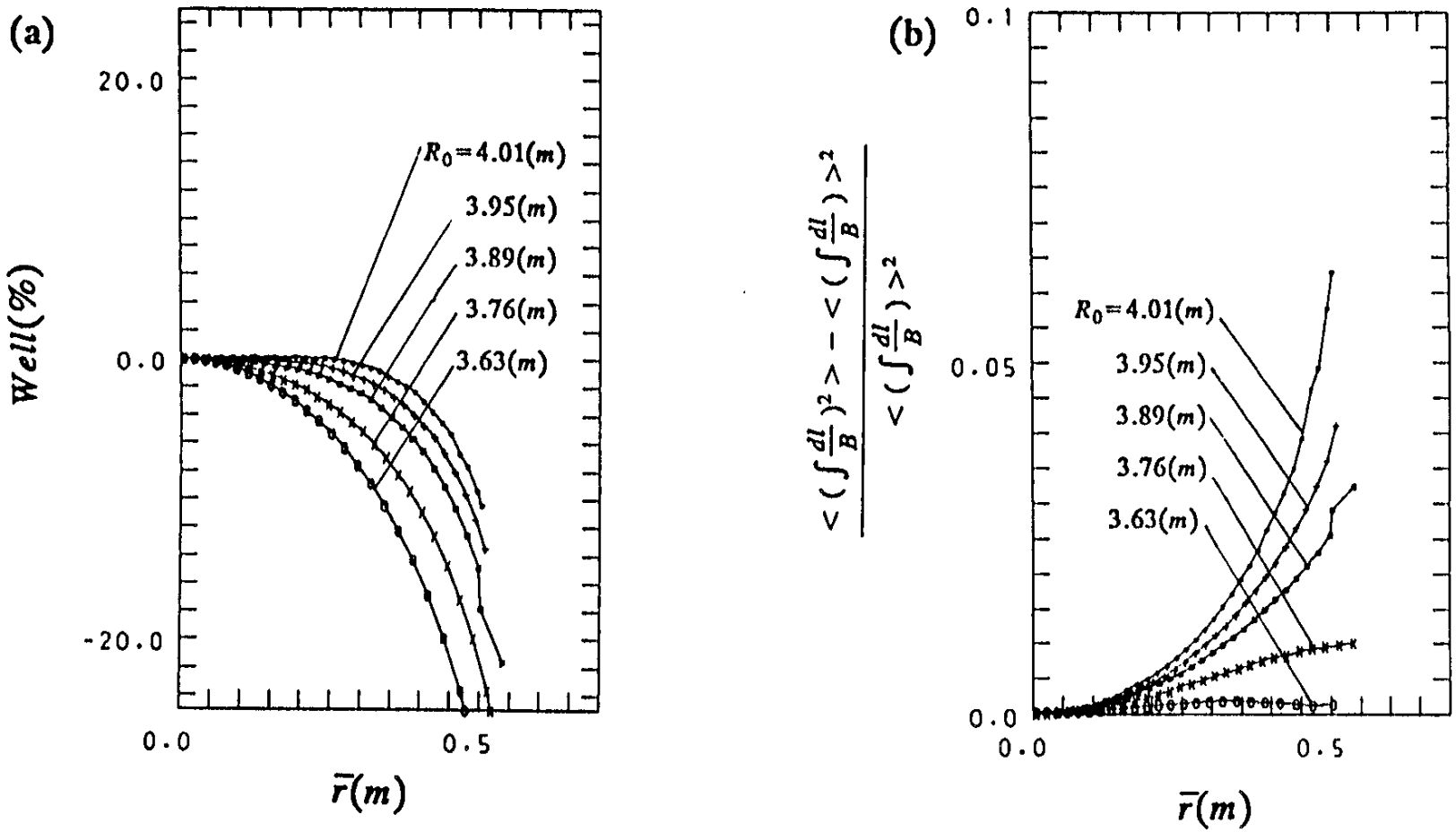

$\bar{\beta}$=0.0(%)

Fig. 4

$\phi = 0°$

$\gamma_c = 1.31$

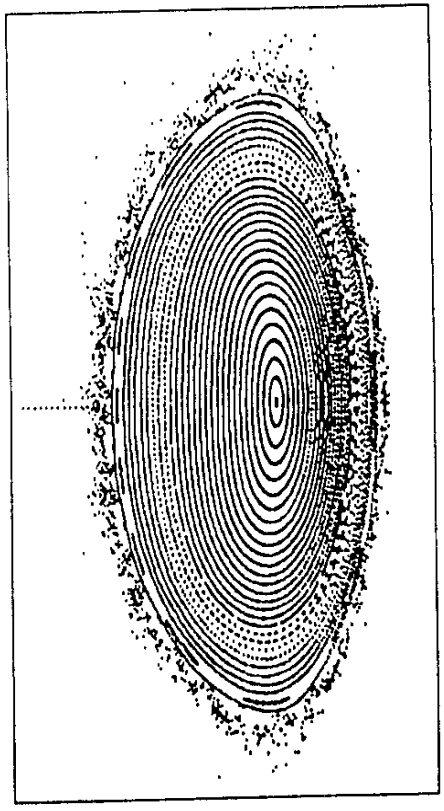

(a) $B_q = 50(\%)$

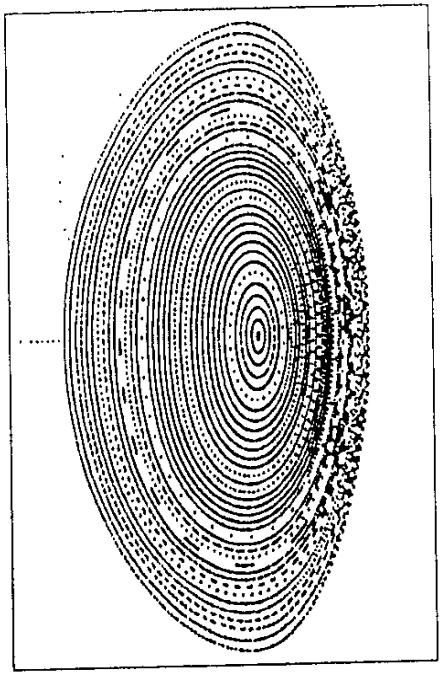

(b) $B_q = 0(\%)$

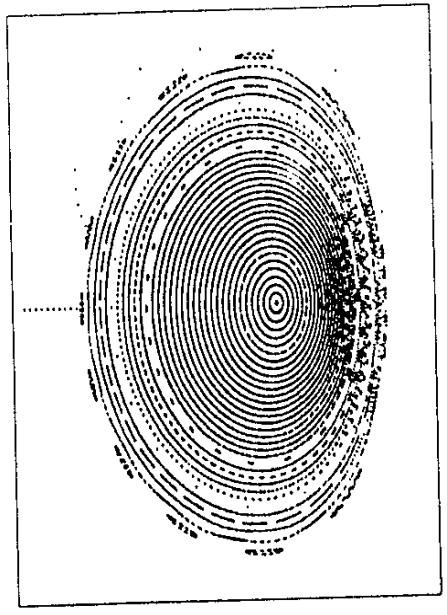

(c) $B_q = -100(\%)$

Fig. 5

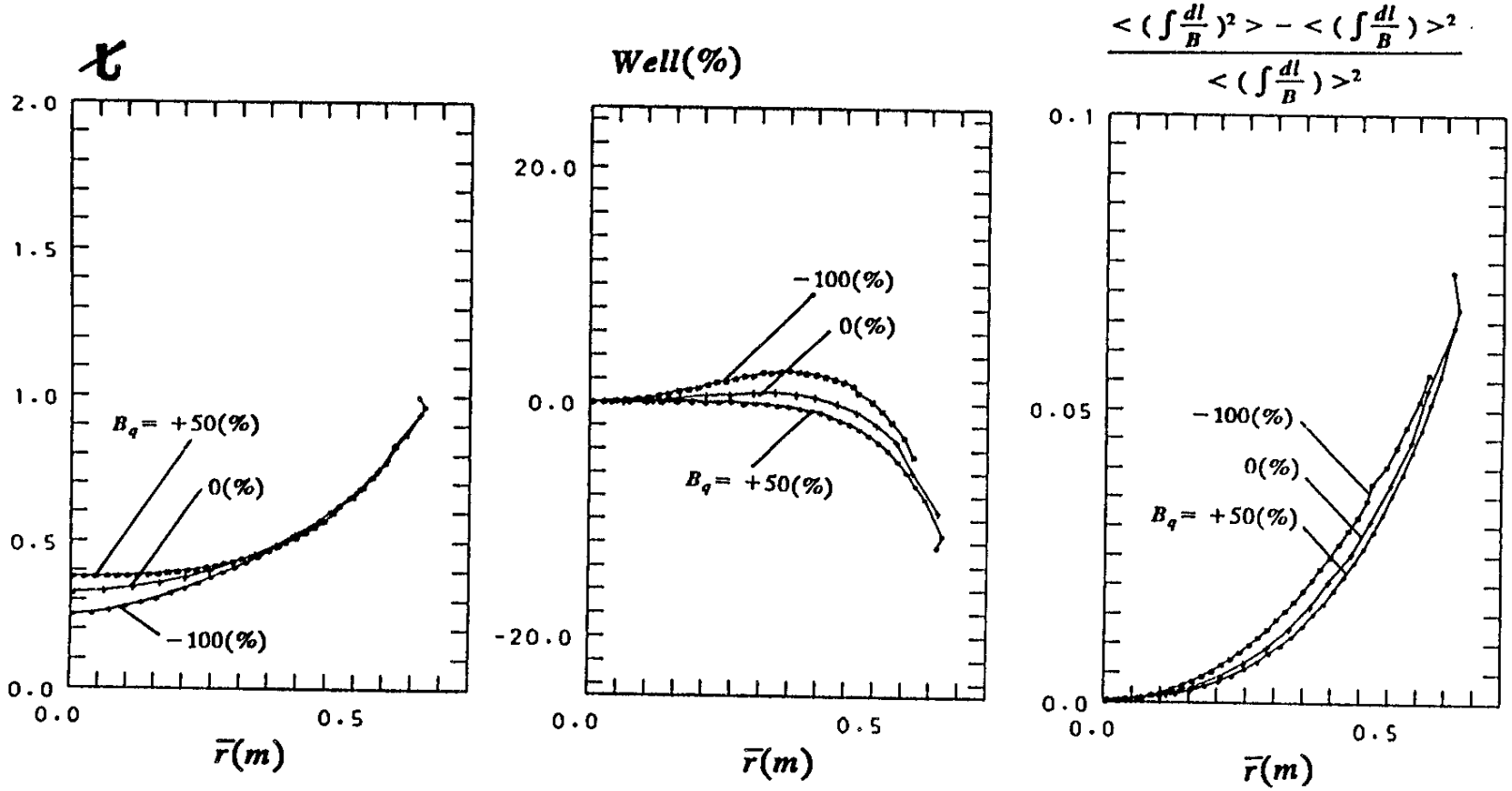

$\bar{\beta}$=0.0(%)

Fig. 6

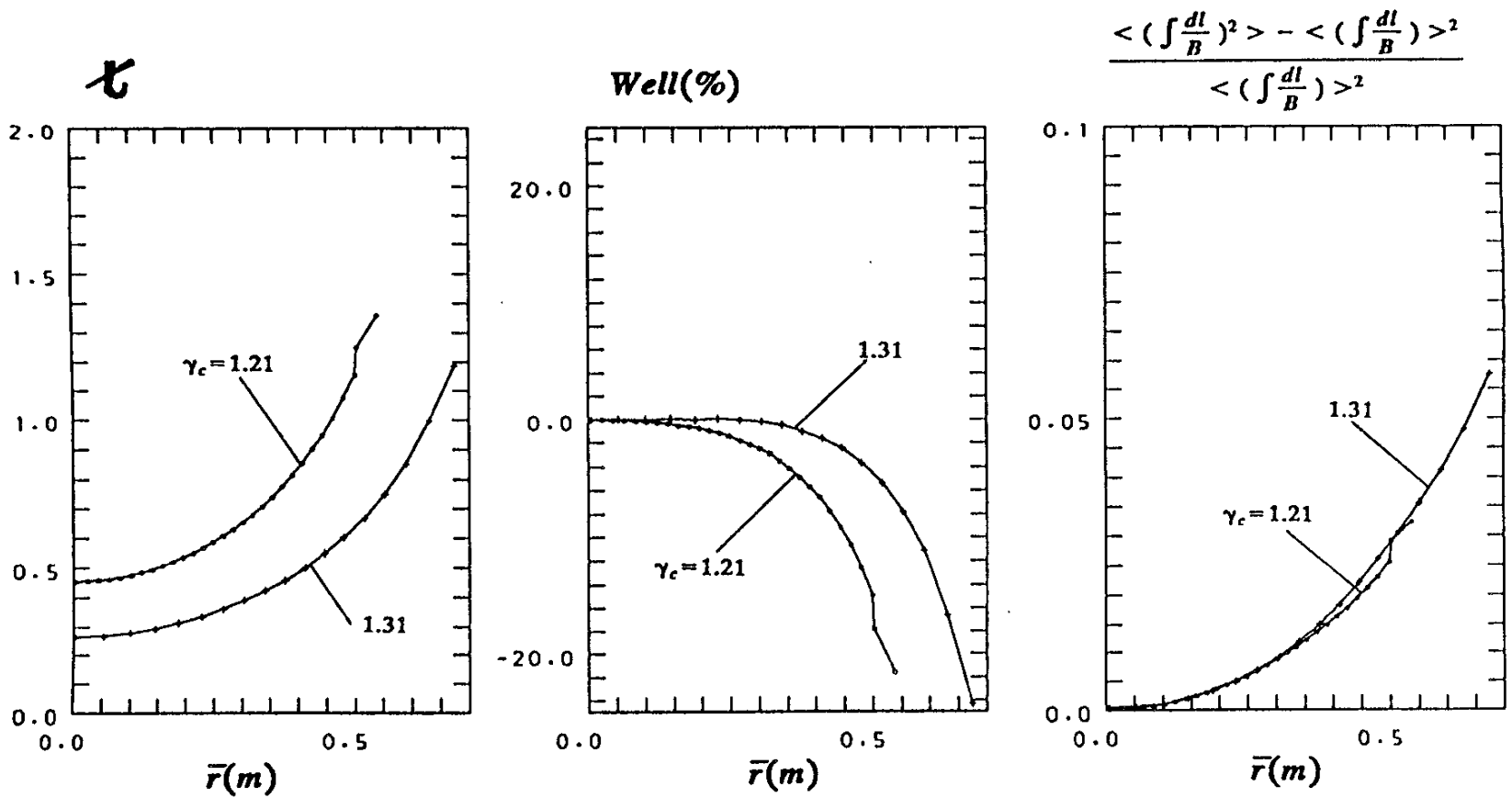

$\bar{\beta}$=0.0(%)

Fig. 7

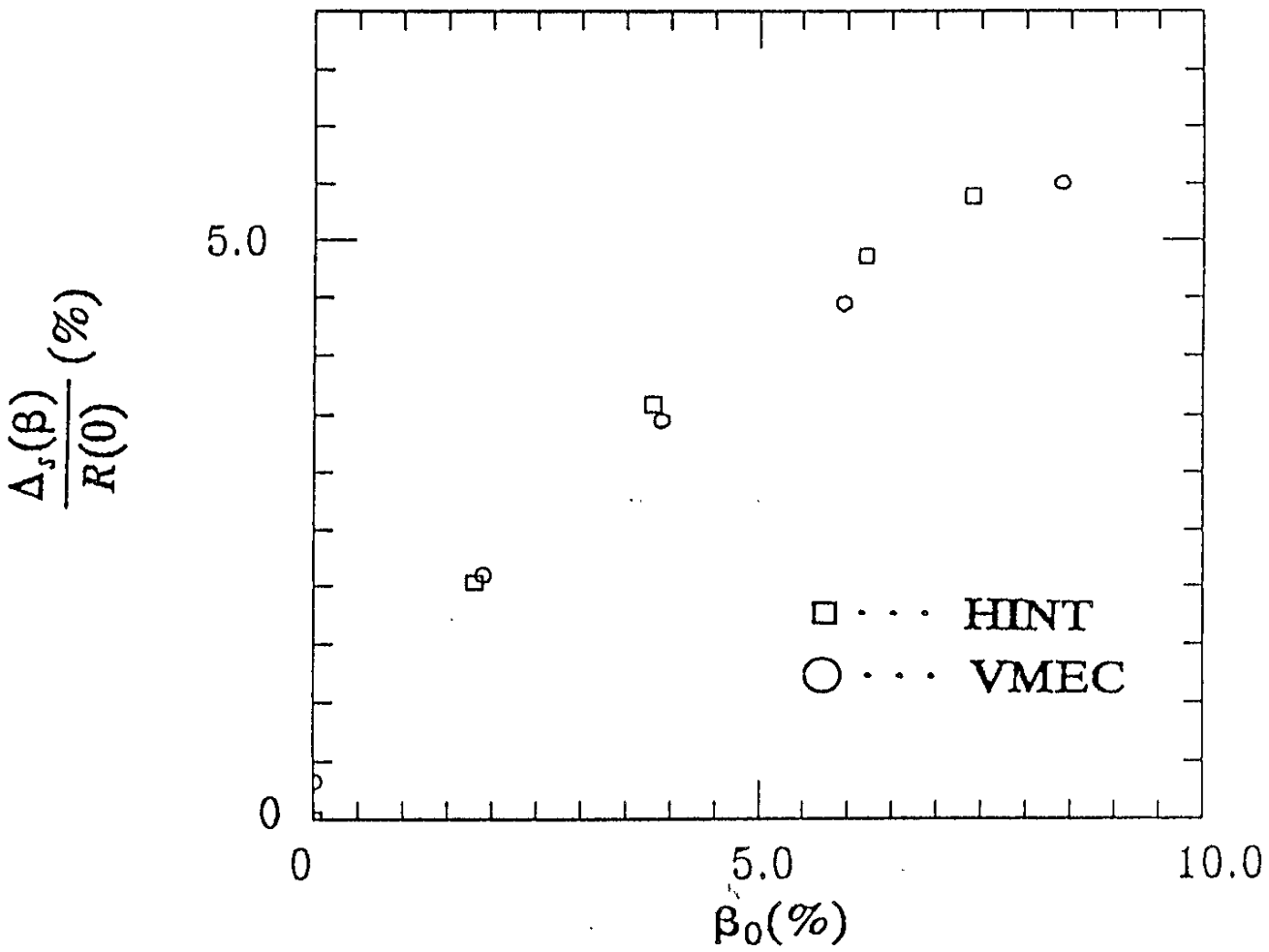

Fig.8

$\phi = 0°$

$\gamma_c = 1.21 \qquad R_0 = 3.76(m)$

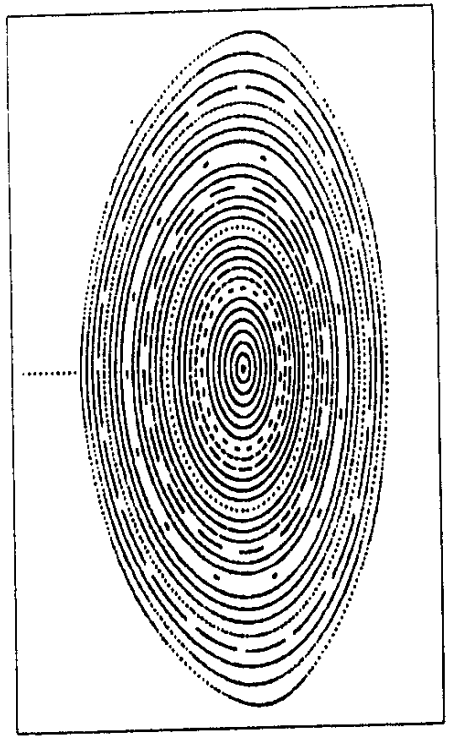

$\bar{\beta} = 0.6(\%)$

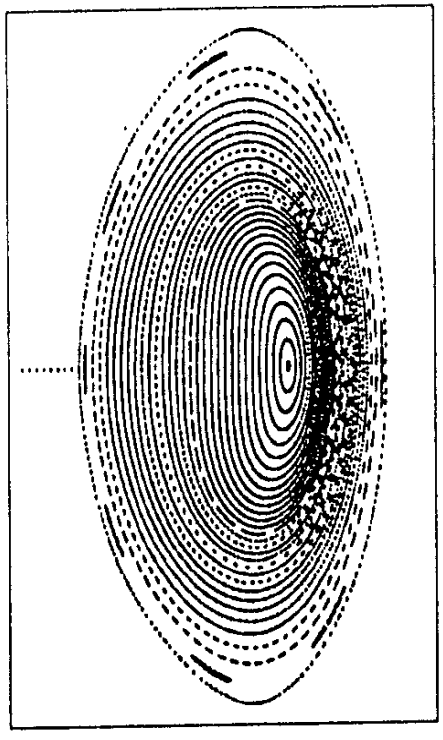

$\bar{\beta} = 2.6(\%)$

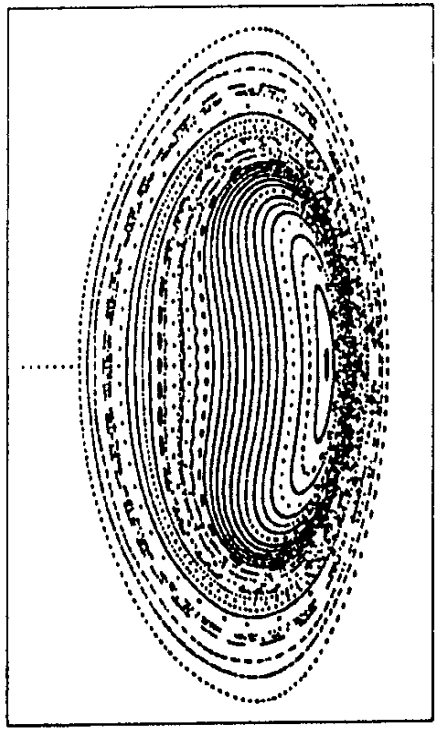

$\bar{\beta} = 5.0(\%)$

Fig. 9

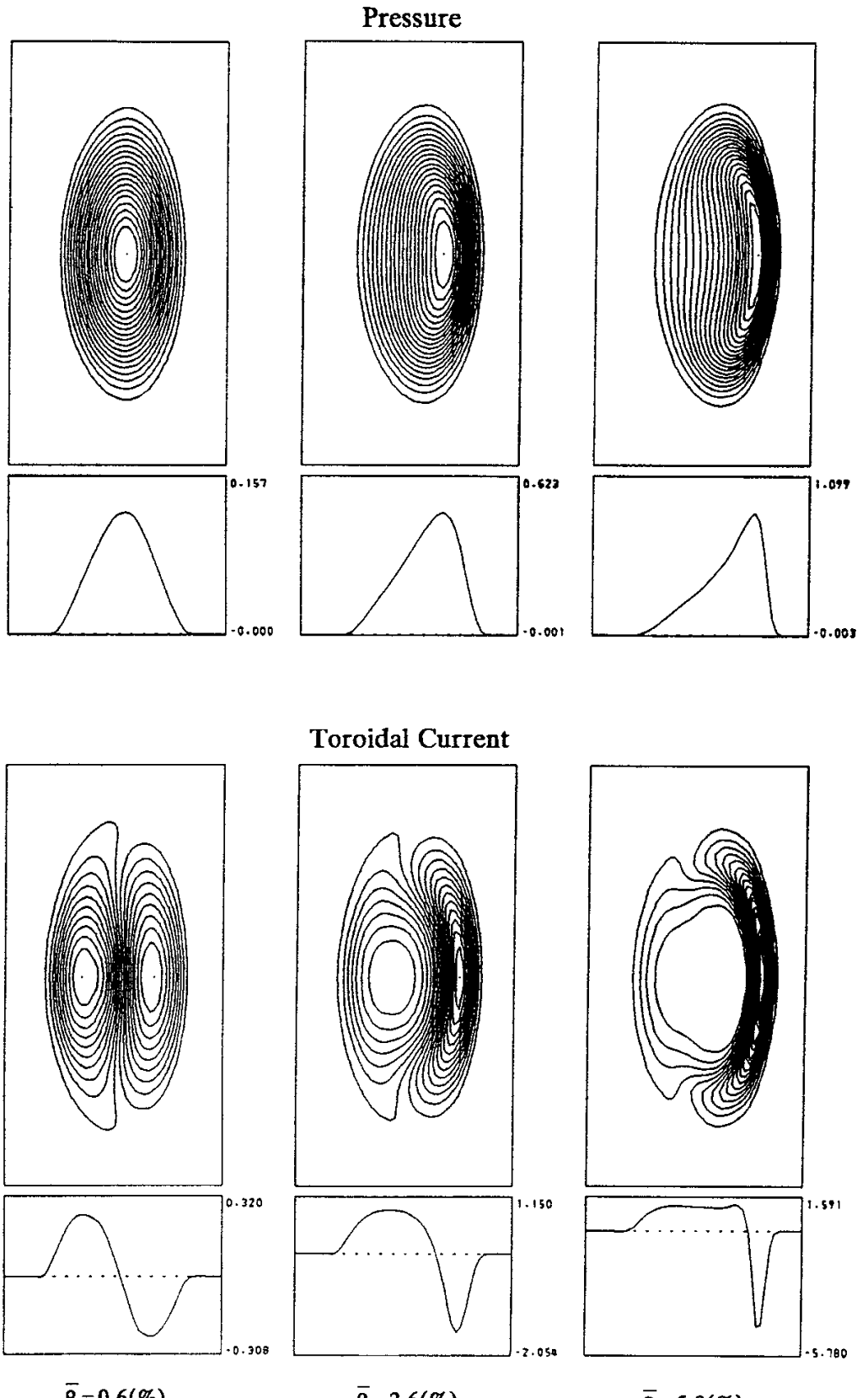
Pressure
0.157
-0.000
0.623
-0.001
1.099
-0.003
Toroidal Current
0.320
-0.308
1.150
-2.054
1.591
-5.780
$\bar{\beta}$=0.6(%)
$\bar{\beta}$=2.6(%)
$\bar{\beta}$=5.0(%)

Fig. 10

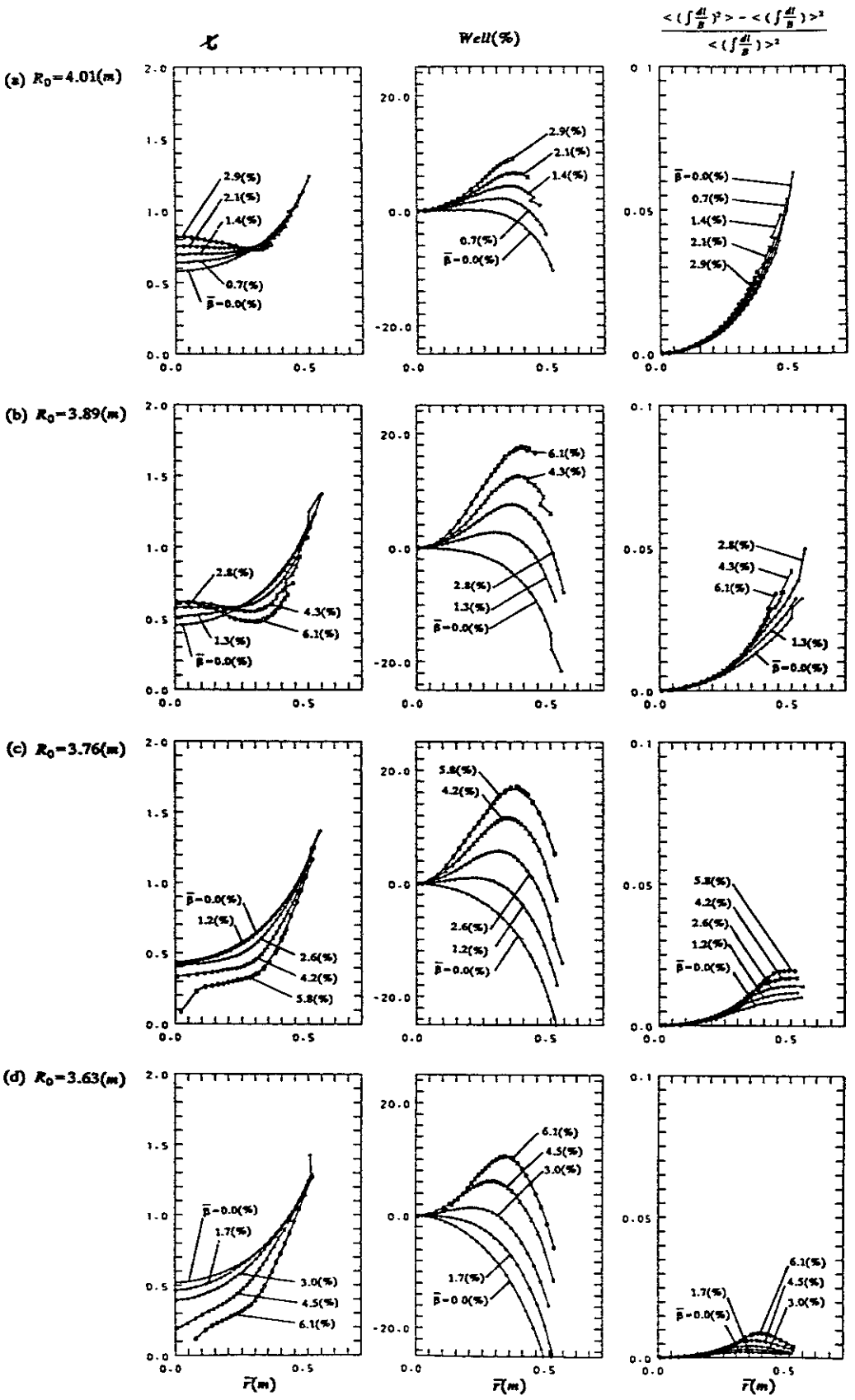
χ
Well(%)
$\frac{<(\int\frac{dl}{B})^2>-<(\int\frac{dl}{B})>^2}{<(\int\frac{dl}{B})>^2}$
(a) R_0=4.01(m)
2.9(%)
2.1(%)
1.4(%)
0.7(%)
β̄=0.0(%)
(b) R_0=3.89(m)
6.1(%)
4.3(%)
2.8(%)
1.3(%)
β̄=0.0(%)
(c) R_0=3.76(m)
5.8(%)
4.2(%)
2.6(%)
1.2(%)
β̄=0.0(%)
(d) R_0=3.63(m)
6.1(%)
4.5(%)
3.0(%)
1.7(%)
β̄=0.0(%)
r̄(m)

Fig. 11

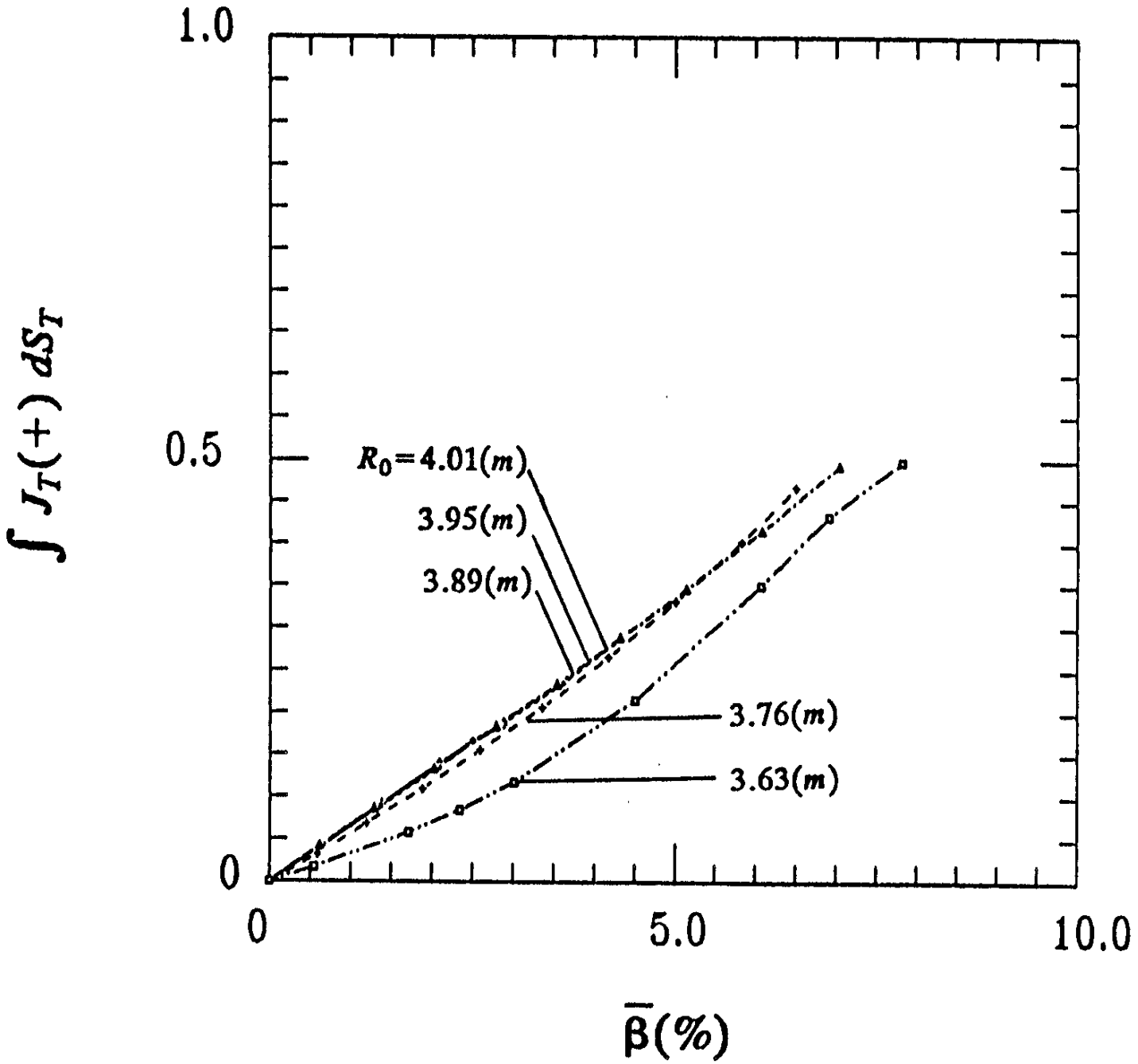

Fig. 12

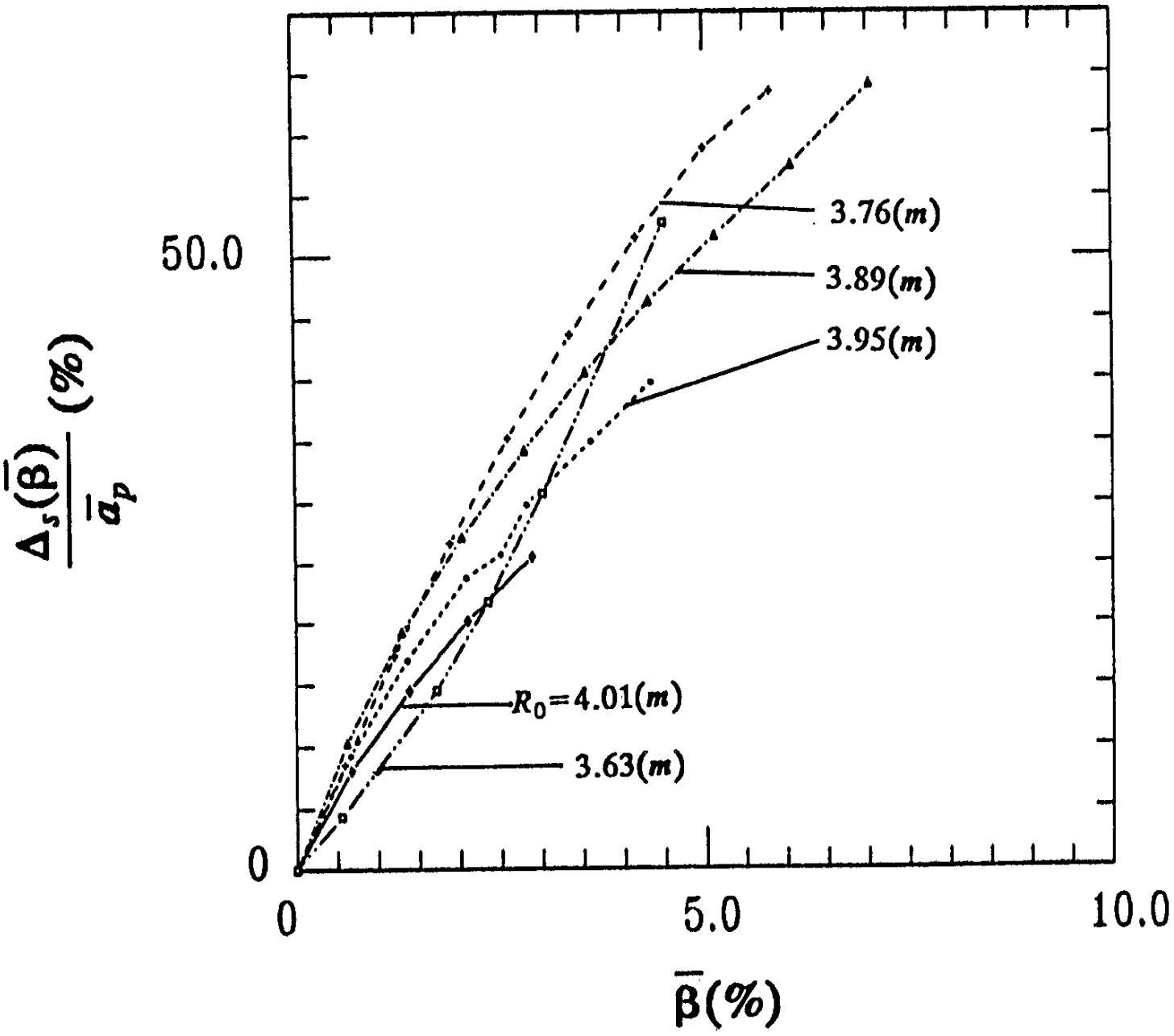
50.0
0
0
5.0
10.0
$\frac{\Delta_s(\bar{\beta})}{\bar{a}_p}$ (%)
$\bar{\beta}$(%)
3.76(m)
3.89(m)
3.95(m)
R_0=4.01(m)
3.63(m)

Fig. 13

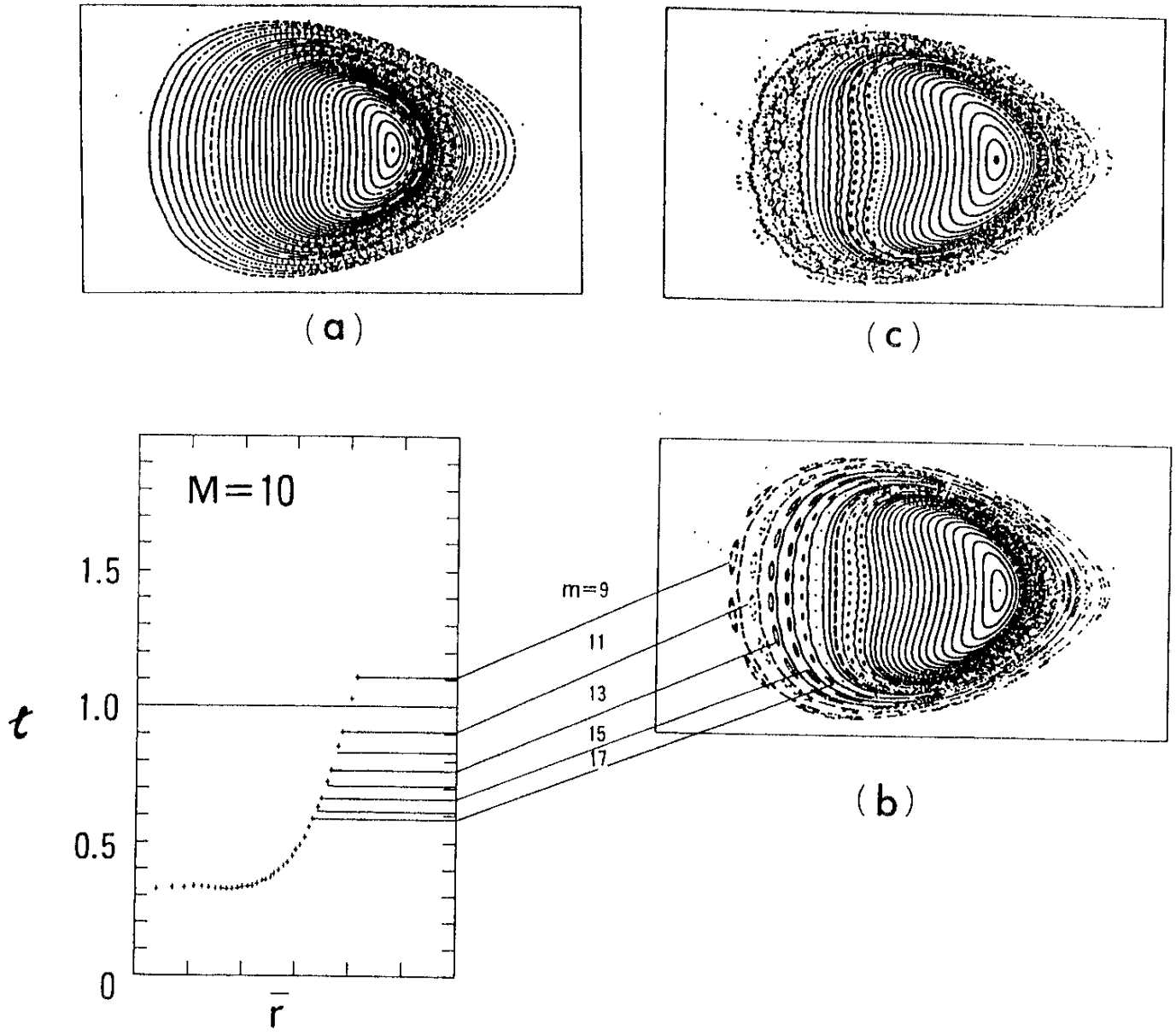

Fig. 14

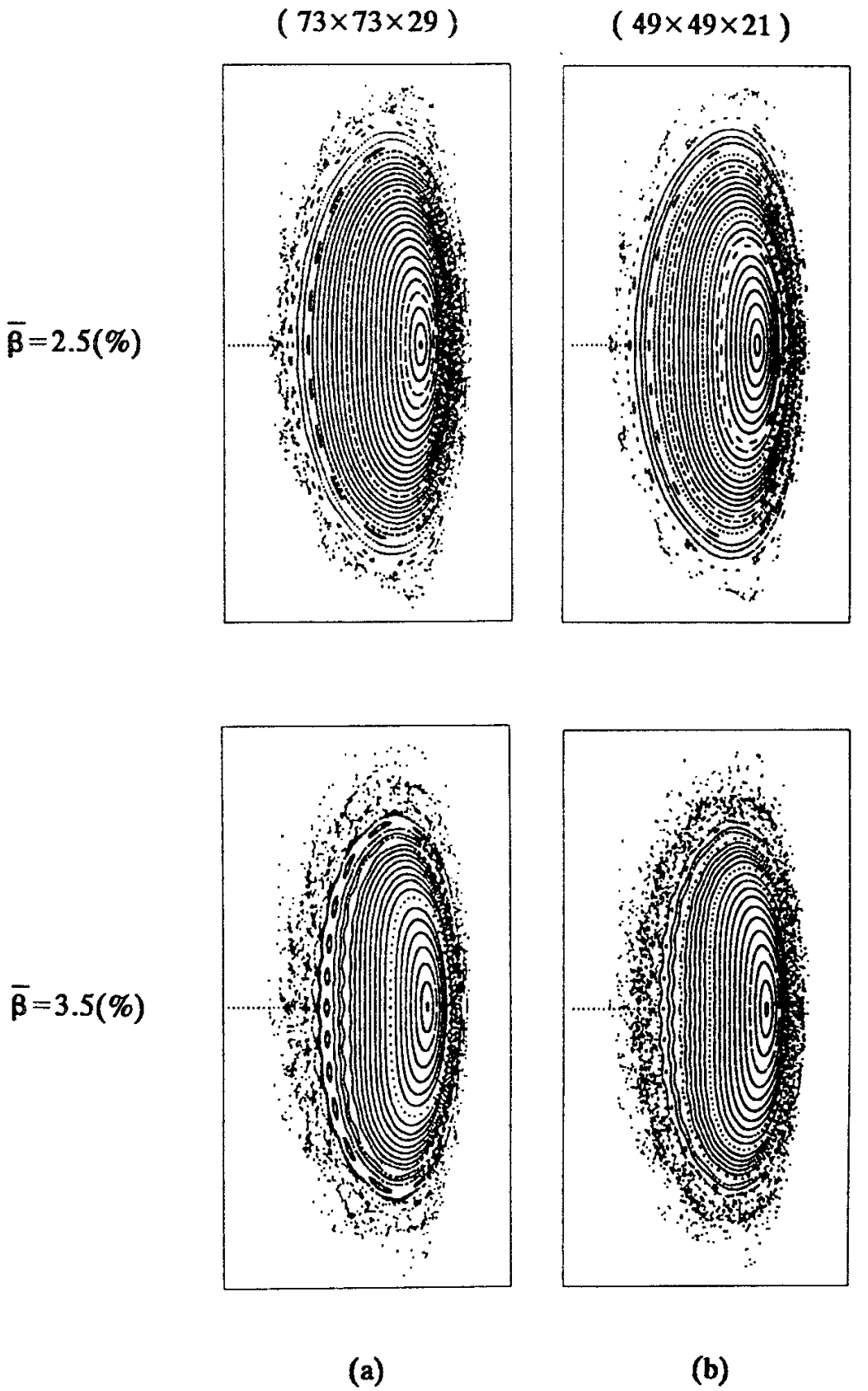

Fig. 15

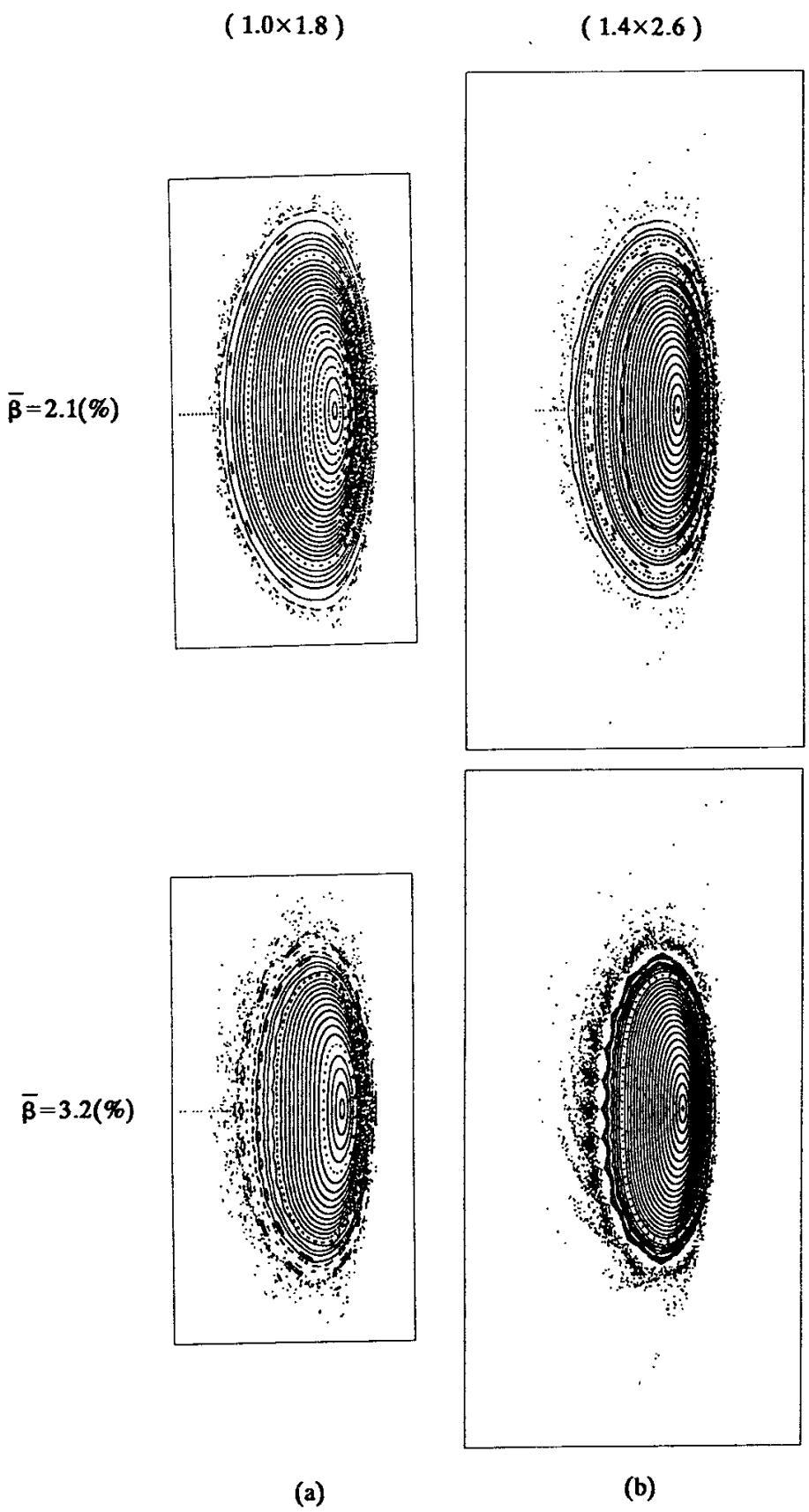

Fig. 16

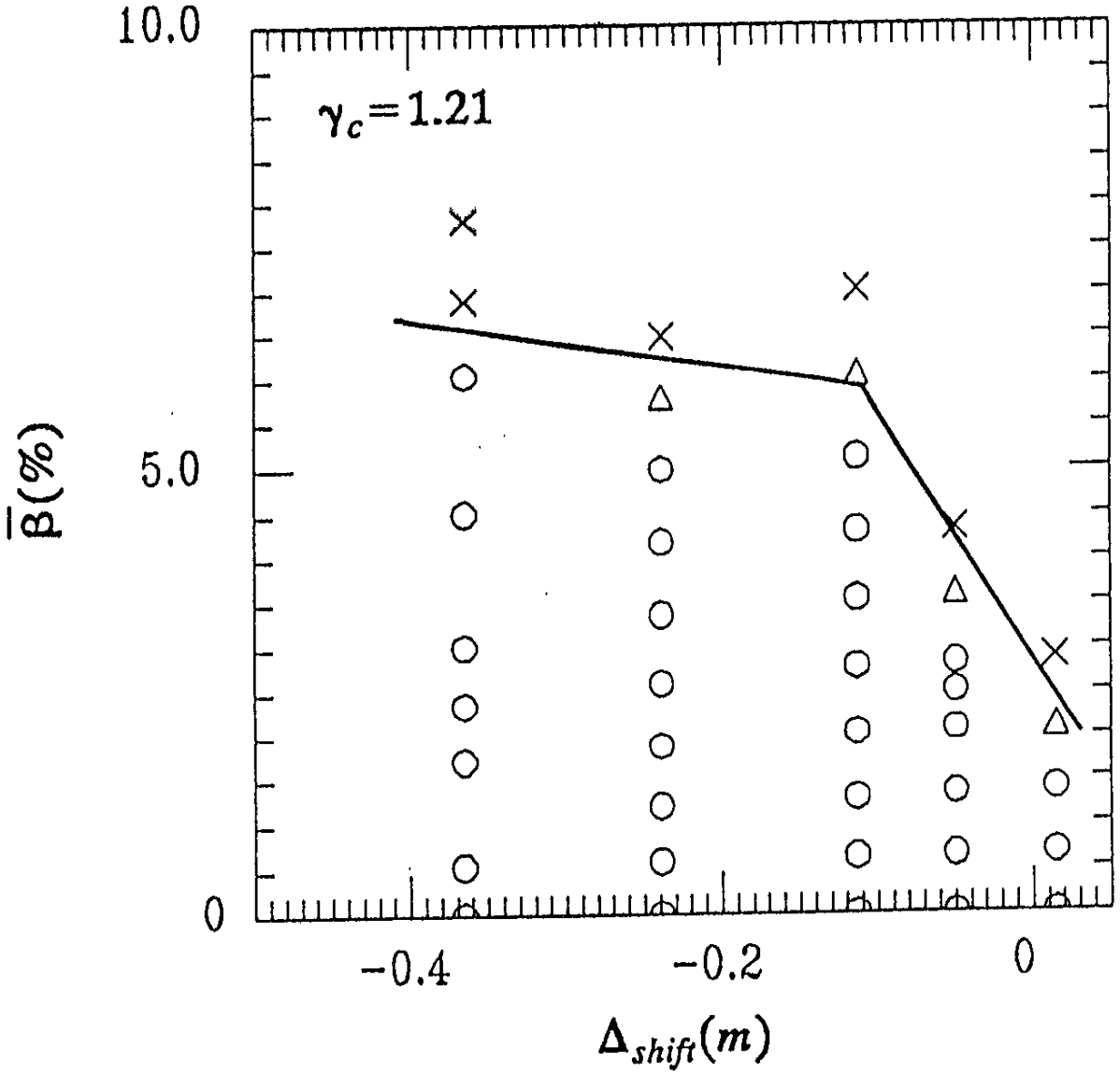

Fig.17

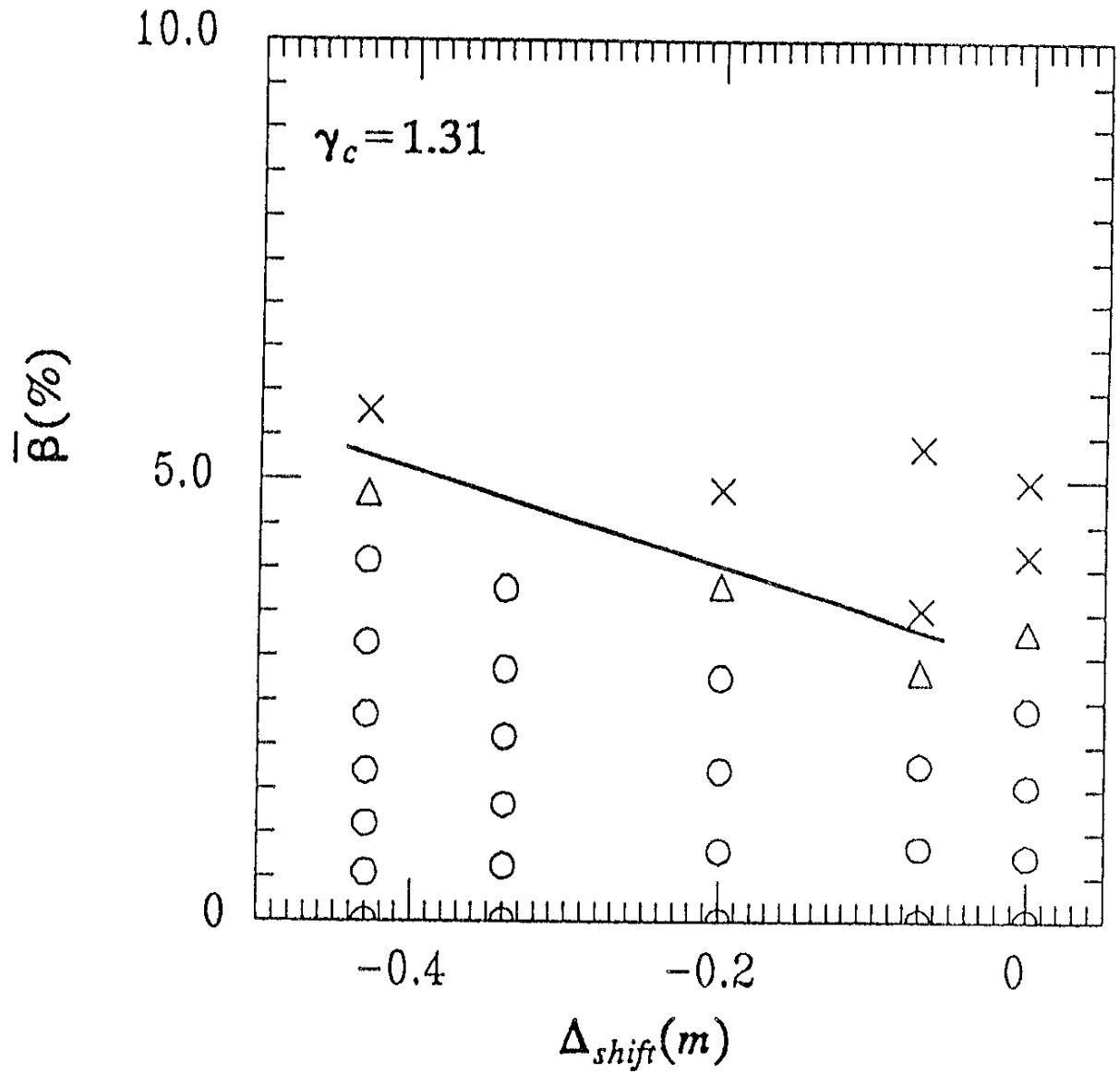

Fig.18

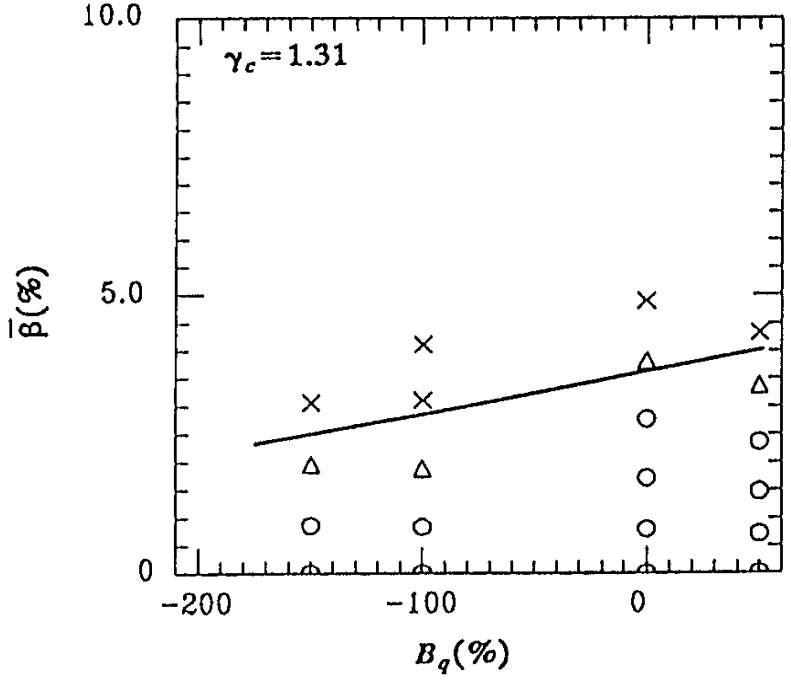

(a) R_0=3.8 (m)

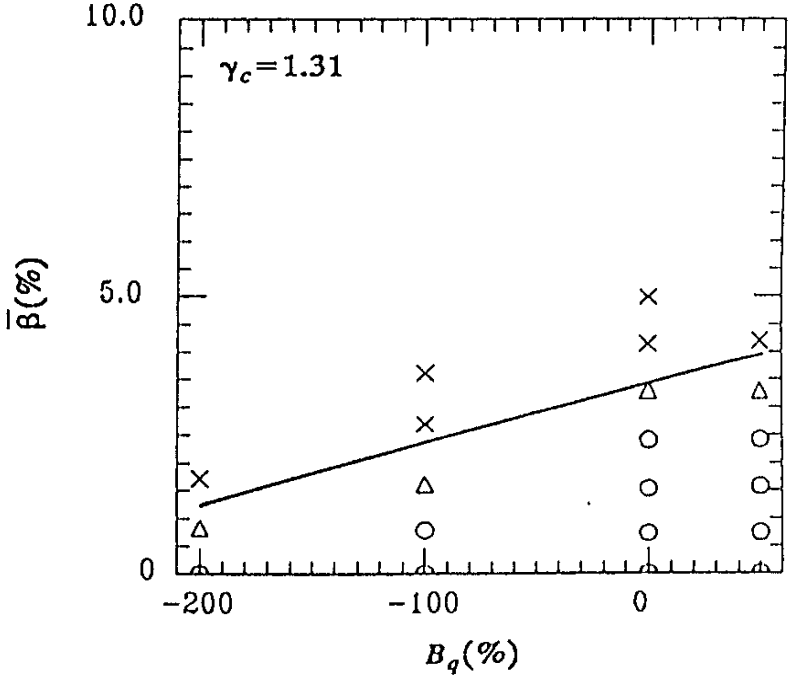

(b) R_0=4.0 (m)

Fig.19